Quantum-mechanical impulse approximation for single ionization of hydrogenlike atoms by multicharged ions

J. E. Miraglia* and J. Macek
University of Tennessee, Knoxville, Tennessee and Oak Ridge National Laboratory, Oak Ridge, Tennessee 37831
(Received 16 July 1990; revised manuscript received 30 January 1991)

A quantum-mechanical approximation is developed for ionization of one-electron targets by charged-ion impact. The model is based on the nonrelativistic distorted-wave formalism valid for impact velocities larger than the electron orbital velocity in the initial state. The exact impulse wave function is used to describe the initial state, thus incorporating the projectile potential to all orders. The final state is represented by a product of continuum Coulomb wave functions around both centers, providing the correct asymptotic conditions and the projectile and target cusps. The theory is thought to be valid for large projectile charge, even larger than the ion velocity. The impulse approximation developed here is expensive in computing time, but it is probably one of the few models to deal with high projectile charges. Double-differential cross sections are computable in the forward and backward ejection angles. Comparisons with the experiments in different regions of interest are presented, including the binary sphere, capture to the continuum cusp, ridge electrons, and backward ejection angles. The theory proves to be quite successful, and it does not seem to deteriorate with increasing projectile charge.

I. INTRODUCTION

In the present work we are interested in the three-particle ionization process:

$$Z_P+(Z_T+e)\rightarrow Z_P+Z_T+e\ , \tag{1.1}$$

where Z_T and Z_P are the target and projectile nuclear charges. Early works on the subject[1,2] demonstrated the importance of the equal status of the Coulomb interactions of both the residual target (T) and the projectile (P) on the outgoing electron (e). During recent years, several distorted-wave methods were put forward to deal with the problem in the perturbation regime, that is, when the ion velocity v is larger than the Coulomb charges Z_T and Z_P. Some theories have proven to be moderately successful—for example, the continuum-distorted-wave[3,4] (CDW), the multiple-scattering[5] (MS), and the eikonal-initial-state[6] (EIS) theories.

In the present work we are interested in the strong-distortion region, that is, when $v \gg Z_T$ and $Z_P \geq v$. In this range no perturbative method successfully describes the details of the angular and energy distributions of the ejected electrons—namely, the double-differential cross section (DDCS). The classical trajectory Monte Carlo[7] (CTMC) is the first approximation that comes to mind to treat such processes. Although the classical theory is known to fail for $v > 5Z_T$ for proton impact, it is observed that the performance of the CTMC improves with Z_P, and so this is a method to compare with in its range of validity. In principle, the close-coupling technique with Sturmian basis sets may also be employed; however, for large Z_P the dimension of the basis to describe the DDCS may be intractable by today's standard.

We are motivated by recent experimental work (Ref. 8), in which energy distributions of ionized electrons in collision between multicharged bare ions and H_2 and He targets have been measured. The bare projectiles used, between C^{6+} and F^{9+} at impact energies between 1 and 2 MeV/amu, places these experiments in the strong-distortion domain. The measurements were done at 0°, ($\theta_e=0$) with respect to the incident beam, where the DDCS exhibits the binary peak. This enhancement is centered near $2v$ in the target frame at $\theta_c=0$ (for any other ejection angle the binary peak centers around $2v\cos\theta_e$). The binary peak can be interpreted as a classical collision between the "quasi-free" target electrons and the projectile (i.e., 180° Rutherford scattering in the projectile frame). By comparing the experiments with the classical model, two major conclusions were drawn in Ref. 8. First, the DDCS of the $2v$ electrons behaves as Z_P^2, as for any first-order perturbative method, and second, some uncertainties arise when the results are normalized to 3-MeV $H^+ + Ne$ K Auger cross section; in this case the experiments were lower than the prediction of the classical binary theory by a factor of approximately 0.6. If true, the corrective factor would indicate a failure not only of the classical theory, but of *any* first-order perturbation theory; in their range of validity, and it is therefore worthy of further study.

Alternatively, the Z_P^2 law has been studied for single-differential cross sections for ionization with CTMC.[7] It was found that for large Coulomb distortion or Sommerfeld parameter Z_P/v, saturation effects, that is, departures from quadratic behavior, occur. For total cross sections, the saturation phenomena are very well known; however, for DDCS the situation is more complex due to the electron capture to continuum (ECC) process which introduces a different Z_P dependence. Saturation was also found theoretically[9] and experimentally[10] in direct

excitation. Therefore, one would expect some indications of such effects in ionization, in particular for slow electrons which can be seen as the continuation of excitation to Rydberg states.[7] In Ref. 8, bare ions of charge $Z_P=6-9$ and velocities $v=6.3-8.9$ were used, and so the corresponding Sommerfeld parameter Z_P/v ranges between 0.95 to 1.4, which is not sufficiently large to observe large saturation effects. Experience with excitation[9] indicates that for $Z_P/v\simeq 1$, departures from the quadratic rule are observable, and so it is interesting to study to what extent saturation effects, *if any,* are relevant for the reported experiments.

Our intention is to develop a theoretical method valid not only for large Z_P but also in the perturbative regime. Any of the three distorted-wave methods cited here—CDW, MS, and EIS—are valid at small Sommerfeld parameters Z_P/v. Any extension to the strong-distortion regime should account for a better description of the *P-e* Coulomb interaction. The mentioned theoretical methods have in common *a product* of continuum wave functions to describe the final channel [see Eq. (2.1) below]. ECC and direct ionization then are described on equal footing, and the Coulomb asymptotic conditions are properly satisfied. These methods differ in the description of the initial channel: MS, CDW, and EIS use plane, peaked impulse [see Eq. (2.16)] and eikonal [see Eq. (2.17)] wave functions, respectively (the MS in second order includes the internuclear interaction in the final, rather than the initial, channel[5]).

The most noticeable effect of the *P-e* interaction in the *exit* channel is the so-called ECC cusp, which is accounted for by the above-mentioned approximations. But in the *entrance* channel the projectile induces a sort of *binding* effect which we have to describe to the best of our abilities if high Z_P are considered.

In the present work, we describe the initial channel by the *exact* impulse wave function[11] [see Eq. (2.5)] which incorporates the projectile potential to all orders, at least on the electron-energy shell. We cannot prove formally that this is the right theory for large Z_P even in the case $v\gg Z_T$. The experience in capture[12] and excitation[13] processes with the exact impulse approximation including the correct asymptotic conditions on both channels, indicates that the method gives a good account of the experiments for asymmetric collision (i.e., when the Coulomb charge of one of the partners is larger than the other one). The price that we have to pay is a three-dimensional numerical integration to obtain the T-matrix element, and an additional two-dimensional one to obtain a DDCS. The quantum theory here formulated will be called simply impulse approximation (IA) and should not be confused with the classical binary model which is often called by the same name. Our goal is to describe the behavior of the ionization DDCS as a function of Z_P using one of the best theoretical treatments without any other approximation than the exact impulse approximation.

Atomic units are used, and the mass of the electron with respect to the heavy nuclei is neglected. As usual, the internuclear interaction was dropped and could be included in an eikonal approximation if we are interested in projectile differential cross sections. In Sec. II, we review the basic formulation. For brevity, the corresponding algebra is not shown: It consists of transforming from position coordinate systems to momentum space, and then using the Nordsieck technique[5,6] to complete the integration. In Sec. III we describe the details of our numerical calculation. A link between the simplest quantum-mechanical approximation and the classical binary theory is presented in the Appendix. From the computational point of view, our formulation is calculable for DDCS in the forward direction where there are three regions of interest—namely, binary electrons at $2v$, ridge electrons around $v/2$, and the ECC cusp or electrons with velocities near to v, which we study in Secs. IV, V, and VI, respectively. The behavior of backward electrons with respect to the projectile direction is studied in Sec. VII.

II. THEORY

The distorted final state is chosen to be a product of functions:

$$\Psi_f^P=\Phi_{\mathbf{K}_T}(\mathbf{R}_T)\psi^-(Z_T,\mathbf{k}_T|\mathbf{r}_T)D^-(Z_P,\mathbf{k}_P|\mathbf{r}_P)$$
$$=\Phi_{\mathbf{K}_P}(\mathbf{R}_P)\psi^-(Z_P,\mathbf{k}_P|\mathbf{r}_P)D^-(Z_T,\mathbf{k}_T|\mathbf{r}_T)\ , \quad (2.1)$$

where

$$\psi^-(Z,\mathbf{k}|\mathbf{r})=\Phi_{\mathbf{k}}(\mathbf{r})D^-(Z,\mathbf{k}|\mathbf{r}) \quad (2.2)$$

is the Coulomb continuum wave function,

$$\Phi_{\mathbf{k}}(\mathbf{r})=\frac{\exp(i\mathbf{k}\cdot\mathbf{r})}{(2\pi)^{2/3}}\ , \quad (2.3)$$

is the normalized plane wave,

$$D^-(Z,\mathbf{k}|\mathbf{r})=\gamma(a)_1F_1(-ia,1,-i\mathbf{k}\cdot\mathbf{r}-ikr)\ ,$$
$$\gamma(a)=\exp(\pi a/2)\Gamma(1+ia)\ , \quad (2.4)$$

$a=\mu Z/k$, and μ is the reduced mass. The usual notation is used: $\mathbf{r}_{T,P}$ are the positions of the electron with respect to the target and projectile, and $\mathbf{R}_{T,P}$ are the corresponding intersystem coordinates. The coordinate systems diagonalizing the kinetic-energy operator are $\{\mathbf{R}_T,\mathbf{r}_T\}$ and $\{\mathbf{R}_P,\mathbf{r}_P\}$. Similarly, $\mathbf{k}_{T,P}$ are the momenta of the electron with respect to the target and projectile. Momenta and positions satisfy the following relation:

$$\mathbf{K}_T\mathbf{R}_T+\mathbf{k}_T\cdot\mathbf{r}_T=\mathbf{K}_P\cdot\mathbf{R}_P+\mathbf{k}_P\cdot\mathbf{r}_P\ .$$

We describe the initial channel within the *exact* impulse approximation:[11]

$$\Psi_i^{\mathrm{IA}}=\int d\mathbf{q}\,\tilde{\phi}_i(\mathbf{q})\Phi_{\mathbf{q}+\mu_T\mathbf{K}_i}(\mathbf{R}_P)\psi^\dagger(Z_P,-\mathbf{k}_i|\mathbf{r}_P)\ , \quad (2.5)$$

where $\mathbf{k}_i=\mathbf{v}-\mathbf{q}$, $\tilde{\phi}_i$ is the Fourier transform of the initial electronic state, $\mathbf{K}_i$ is the momentum of the projectile with respect to the target,

$$\mu_T^{-1}=(M_T+1)^{-1}+(M_P)^{-1}$$

is the electron-target reduced mass, and M_T and M_P are

the target and projectile masses, respectively.

The T-matrix element is given by

$$T_{\rm IA}=\langle\Psi_f^P|V_f|\Psi_i^{\rm IA}\rangle=\langle\Psi_f^P|V_i|\Psi_i^{\rm IA}\rangle\ ,$$

where the final and initial potentials satisfy $(H-E)\Psi_f^P=V_f\Psi_f^P$ and $(H-E)\Psi_i^{\rm IA}=V_i\Psi_i^{\rm IA}$; H and E are the Hamiltonian and the total energy, respectively. After using the Nordsieck technique and some algebra, we find that $T_{\rm IA}$ is given by

$$T_{\rm IA}=-\frac{4}{(2\pi)^3}\int d\mathbf{q}\frac{\tilde V_T(\mathbf{P})C(a_T,A_T)}{A_T}\frac{\tilde V_P(\mathbf{P})C(a_P,A_P)}{A_P}\times\frac{\mathbf{Q}\cdot\mathbf{V}}{Q^4}C(a_i,A_i)\tilde\phi_i(\mathbf{q})\ , \tag{2.6}$$

where the tilde denotes the Fourier transform

$$\tilde V_{T,P}(\mathbf{P})=-\left[\frac{2}{\pi}\right]^{1/2}\frac{Z_{T,P}}{P^2}\ , \tag{2.7}$$

$$\mathbf{P}=\mathbf{K}_i-\mathbf{K}_T,\quad p=|\mathbf{P}|,\quad \mathbf{Q}=\mathbf{P}-k_T+\mathbf{q}\ , \tag{2.8}$$

$$C(a,A)=\gamma(a)A^{-ia}\ , \tag{2.9}$$

$$a_i=Z_P/k_i,\quad a_P=Z_P/k_P,\quad a_T=Z_T/k_T\ , \tag{2.10}$$

$$\begin{aligned}A_P&=1+\frac{2}{p^2+\epsilon^2}(-\mathbf{P}\cdot\mathbf{k}_P-ik_P\epsilon)\ ,\\ A_i&=1+\frac{2}{p^2+\epsilon^2}(-\mathbf{P}\cdot\mathbf{k}_i-ik_i\epsilon)\ ,\\ A_T&=1+\frac{2}{Q^2+\epsilon^2}(+\mathbf{Q}\cdot\mathbf{k}_T-ik_T\epsilon),\quad \text{as } \epsilon\to0^+\\ A_3&=1+\frac{2}{p^2+\epsilon^2}(k_ik_P-\mathbf{k}_i\cdot\mathbf{k}_P)\ ,\end{aligned} \tag{2.11}$$

$$\mathbf{V}=Y_2k_i\hat{\mathbf{k}}_P-Y_2\mathbf{k}_i-Y_1\mathbf{P}\ , \tag{2.12}$$

$$Y_2=\frac{ia_i}{A_i}F^+\ ,\quad Y_1=\frac{A_i-A_3}{A_p}Y_2-F\ , \tag{2.13}$$

$$\begin{aligned}F&={}_2F_1(ia_1,ia_P,1,X)\ ,\\ F^+&={}_2F_1(1+ia_1,1+ia_P,2,X)\ ,\end{aligned} \tag{2.14}$$

and

$$X=1-\frac{A_P+A_i-A_3}{A_pA_i}\ . \tag{2.15}$$

Although the expression for the matrix element $T_{\rm IA}$ is complicated, its interpretation is simple: The electron initially bound, represented by a wave packet $\tilde\phi_i(\mathbf{q})$, is distorted by the incoming projectile through $C(a_i,A_i)$. In the final channel, both the residual target and the projectile distort the outgoing electron via $\tilde V_T(\mathbf{P})C(a_T,A_T)A_T^{-1}$ and $\tilde V_P(\mathbf{P})C(a_P,A_P)A_P^{-1}$, respectively, on equal footing. It is important to note that Eq. (2.6) is valid for *any* initial electronic state. The Fourier transform of the initial state, namely, $\tilde\phi_i(\mathbf{q})$, provides the initial electron momentum distribution.

Equations (2.1) and (2.5) are written in such a way that most theoretical approximations emerge with specific choices of parameters.

(a) If $Z_T=Z_P=0$ in Eq. (2.1) and $Z_P=0$ in Eq. (2.5), we obtain the plane-wave approximation,[14] which is closely related to the binary classical theory (see the Appendix for details).

(b) If $Z_P=0$ in Eq. (2.1) and $Z_P=0$ in Eq. (2.5), we obtain the first-order Born approximation considered as a direct process, as reported by Bates and Griffing.[15]

(c) If $Z_T=0$ in Eq. (2.1) and $Z_P=0$ in Eq. (2.5), we obtain the first-order approximation considered as a capture to the continuum process, as reported by Dettmann.[16]

(d) If $Z_P=0$ in Eq. (2.5), we obtain the first-order multiple-scattering approximation.[5]

(e) If $\mathbf{k}_i=\mathbf{v}$ in Eq. (2.5), we obtain the CDW approximation.[4] The initial wave function is then the *peaked* version of the IA, Eq. (2.5), given by

$$\Psi_i^{\rm CDW}=\Phi_{\mathbf{K}_i}(\mathbf{R}_T)\phi_i(\mathbf{r}_T)D^\dagger(Z_P,-\mathbf{v}|\mathbf{r}_P)\ . \tag{2.16}$$

(f) If $\mathbf{k}_i=\mathbf{v}-\mathbf{P}+\mathbf{k}_T$ in Eq. (2.5), we obtain the modified CDW approximation.[17]

(g) If in Eq. (2.16), we approximate the Coulomb distortion $D^\dagger(Z_P,-\mathbf{v}|\mathbf{r}_P)$ by its long-distance limit,[6] we obtain $\Psi_i^{\rm EIS}$,

$$\Psi_i^{\rm EIS}=\Phi_{\mathbf{K}_i}(\mathbf{R}_T)\phi_i(\mathbf{r}_T)\exp\left[-i\frac{Z_P}{v}\ln(vr_P+\mathbf{v}\cdot\mathbf{r}_P)\right]\ . \tag{2.17}$$

(h) If $Z_P=0$ or $Z_T=0$ in Eq. (2.1), we obtain the exact prior impulse approximation for ionization considered as a direct or capture process, respectively. It should also be noted that the IA for capture with $Z_P/v>1$ is essentially equivalent to the distorted-wave strong-potential Born approximation (DSPB).

The first seven theoretical methods cited above have T-matrix elements that can be expressed in closed forms, and this is a great advantage because, by making the corresponding approximations at the level of the integrand, we can test our numerical procedure. When $Z_P/v\ll1$, we can approximate $\mathbf{k}_i\sim\mathbf{v}$, and the present IA should tend to the CDW.

The PW approximation is the simplest quantum model. The T-matrix element and DDCS (in the forward direction) can be obtained in closed form (see the Appendix). It behaves as Z_P^2. The EIS represents the next level of sophistication. Its T-matrix element has closed form in terms of the hypergeometric functions ${}_2F_1$, and the DDCS requires a numerical integration. The correct asymptotic conditions are satisfied in both the initial and final channels, and higher orders in Z_P are included through the distorted-wave formalism. The EIS is certainly one of the most successful models used so far in the perturbative regime.[18] The IA developed here represents a further step forward toward dealing with high Z_P. The numerical computation is quite laborious, but it is perhaps the only quantum-mechanical model appropriate for ionization by multicharged ions. In the present work we compare IA results with those of the PW (dotted lines throughout the figures) and EIS (dashed lines) to see the

differences with the simplest first-order and a current distorted-wave method, respectively.

The double-differential cross section reads, in general,

$$\frac{d\sigma}{dE_e d\Omega_e} = \int d\Omega \frac{d\sigma}{dE_e d\Omega_e d\Omega} , \tag{2.18}$$

where

$$\frac{d\sigma}{dE_e d\Omega_e d\Omega} = \frac{2\pi k_T}{\mu_T^2 v^2} |T|^2 ,$$
$$\mu_T^{-1} = (M_T+1)^{-1} + (M_P)^{-1} , \tag{2.19}$$

$d\Omega = \sin\theta \, d\varphi \, d\theta$, φ and θ are the azimuthal and polar angles of the scattered projectile, and $d\Omega_e = \sin\theta_e d_{\varphi e} d\theta_e$ is the differential solid angle of the ejected electron in the target frame.

III. DETAILS OF THE NUMERICAL CALCULATION

In this work we make *no* further approximations. All the integrations have been carried out numerically. Some computational limitations should be mentioned. The three-dimensional integrals on $\mathbf{q}(\varphi_q, \theta_q, q)$ were performed with a relative error ϵ_r much less than 1%, 1.5%, and 2% for φ_q, θ_q, and q, respectively. The modulus square of the T-matrix element then is obtained with $\epsilon_r \ll 0.04$. The integration on the projectile angular distribution θ was estimated to introduce an additional 1% of uncertainty. So we conclude that the present results have a numerical relative error of less than 5%.

Most of the computing time is spent in the calculation of the two hypergeometric functions ${}_2F_1$. When analytic continuation is needed, the task becomes more complicated because in this case four functions ${}_2F_1$, besides the corresponding Γ functions are required. The function ${}_2F_1$ was obtained with only four significant figures. The convergence of the usual series representing the hypergeometric function is very slow when a_i and/or a_P are large. The situation is aggravated for large Z_P.

As $Q \to 0$, the factor A_T tends to zero and there $C(a_T, A_T)$ introduces infinite oscillations, typical of Coulomb distorted-wave functions. As usual, to avoid the infinite oscillations, we use a cutoff $\epsilon \sim 10^{-4}$ instead of the mathematical limit as $\epsilon \to 0+$. Note that when $Q=0$, we have the momentum conservation equation for a given value of $\mathbf{q}$, namely, $\mathbf{P} - \mathbf{k}_T + \mathbf{q} = 0$, or $\mathbf{K}_i + \mathbf{q} = \mathbf{K}_T + \mathbf{k}_T$.

In this work we present DDCS results in the forward and nearly forward directions. In this case, the integration on the projectile azimuthal φ is straightforward and the task is reduced to a four-dimensional integral. This is work that can be done with today's computers: One DDCS requires about 1 h of CPU time in a cluster composed of a Vax 8800 and a 6000-440. A total cross section would require a seven-dimensional numerical integration, which would be a formidable task. T-matrix elements in the EIS and CDW approximations have closed forms and can be performed very quickly (say 1 sec, per DDCS) in comparison with the IA calculation.

The theory developed here deals with purely hydrogenic targets. To extend it to two-or-more-electron targets, we need to make some approximations, viz., (i) H_2 targets were considered to be composed of two hydrogenic atoms with $Z_T = 1.065$ to satisfy the experimental binding energy of 15.4 eV. (ii) He targets were considered as two-independent-electron targets. The *initial* bound state was described by the 5-z wave function of Clementi and Roetti,[19] with binding energy 24.9 eV, and the target change in the *final* continuum state was taken to be 1.687 (Ref. 20) in order to make this distorted wave as orthogonal as possible to the initial orbital.

Another point of interest is that the final perturbation was used, i.e., V_f. In the case of hydrogenic targets, the use of V_i or V_f gives the same result, but this is not the case when dealing with multiple-electron systems. These approximations, which are common to most of the theories are stated here explicitly to permit reproduction of the present results and comparisons of the different theories on an equal basis.

IV. BINARY ENCOUNTER PEAK OR $2v$ ELECTRONS

As defined before, $2v$ binary electrons are those electrons ejected in the forward direction, attributed mainly to head-on collisions with the projectile. In the following paragraphs we will be interested in three features, viz., saturation, shape, and position of the binary peak.

A. Saturation

Our bench mark here is the measurement of multicharged bare projectiles on H_2 at 1.5-MeV/amu impact energy ($v = 7.746$), where the binary encounter peaks at around 3168 eV in the target frame, or 770 eV in the projectile frame, corresponding to $k_T \sim k_{TM} = 15.26$. DDCS results are presented in Fig. 1 as a function of Z_P for k_{TM} in the forward direction along with the experiments.[8] First-order PW and Born approximations behave as 3×10^{-23} and $2.9 \times 10^{-23} Z_P^2$ cm^2/eV sr, respectively, and both account well for the data. The EIS approximation also follows the experiments in the low-charge domain. For $Z_P = 9$, EIS coincides with first Born results and it is 3% below the PW. For the same projectile charge, the IA is 8% below the PW approximation. No conclusion can be drawn because the IA is well within the numerical and experimental uncertainties. For large Z_P, the situation changes: the IA approximation exhibits a clear saturation, which is also present in the EIS, but less prominently. The full meaning of this departure from the Z_P^2 behavior will be appreciated in the next Secs. IV B and IV C when we study the shape and the peak position.

We can conclude that EIS, and even the PW approximations, can be used when $Z_P < 15$ in our case [say, $Z_P < 2(v/Z_T)$ in general] and there is no need to introduce more sophisticated and expensive models. These approximations could be used then to study the binary peak production with an increasing number of projectile

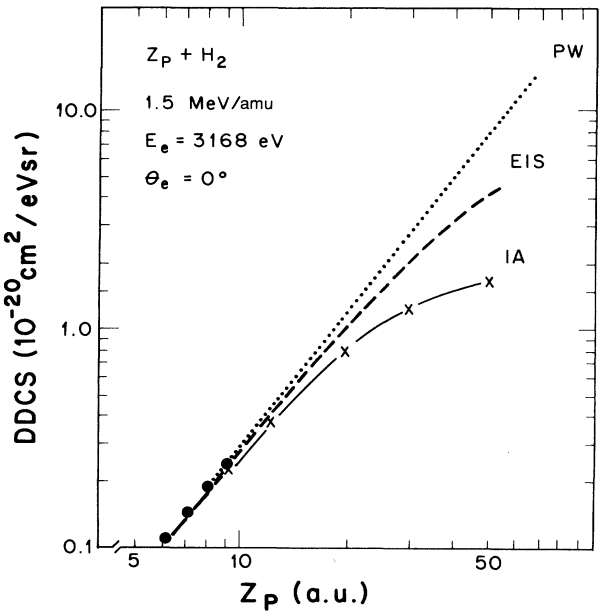

FIG. 1. Double-differential cross sections in the forward direction ($\theta_e=0$) for ionization of H_2 by impact of bare ions as a function of the projectile charge. The electron energy is 3.168 keV (or $k_T=15.26$) and the impact energy is 1.5 MeV/amu ($v=7.746$). All quantities are in the target reference frame. Theory dotted and dashed lines denote the PW and EIS approximations, respectively, and the crosses are the calculations with the present IA (the solid lines connecting the crosses are only to guide the eye). The solid circles are the experiments from Ref. 8.

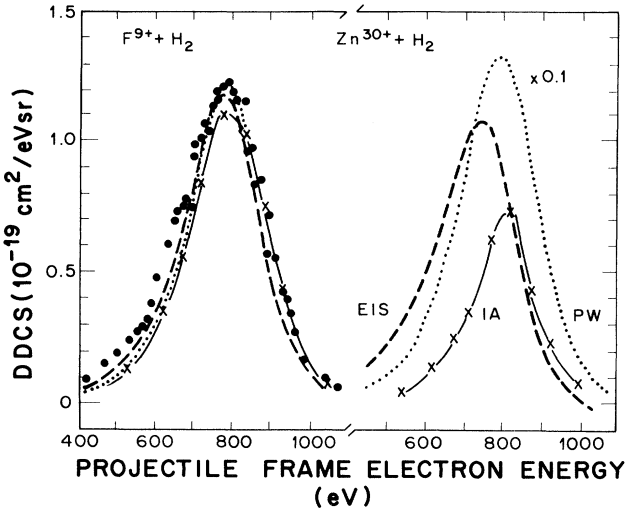

FIG. 2. Double-differential cross section in the projectile frame in the forward direction ($\theta_e=0$) for ionization of H_2 by impact of bare ions F^{9+} and Zn^{30+} as a function of the projectile-frame electron energy. The impact energy is 1.5 MeV/amu ($v=7.746$). Results of Zn^{30+} are divided by ten. Theory as in Fig. 1, and solid circles are the experiments as reported in Ref. 8 i.e., normalized to the classical binary theory).

electrons, where the cross section was found to increase as the total projectile charge decreases.[21]

B. Shape

As shown in the last paragraph, there are no large deviations from the Z_P^2 law for the binary encounter peak in the cases studied in Ref. 8., and so we can use any first-order theory to delineate its form. In Fig. 2(a) we show the PW and EIS approximations for F^{9+} on H_2 and compare with the experiments. The agreement is good. The IA, also shown in the figure, is about 8% below at the maximum and exhibits a small skewness favoring the high-energy electrons. If we normalized the experiments to the IA (in Ref. 8 the data were normalized to the classical binary theory), it would not be possible to reach a firm conclusion about its performance because of the experimental and numerical uncertainties.

As Z_P increases, the binary peak starts to be distorted by the projectile, and higher orders in Z_P are certainly needed. To illustrate this situation, we have chosen $Z_P=30$ at the same impact velocity. Figure 2(b) shows the PW; EIS, and IA approximations. Here, it is clear that two effects occur: First, the peak is *relatively* broadened, and second, the position of the maximum is shifted relative to the first-order PW approximation. Remarkably, the IA favors higher electron energies in contrast with the EIS prediction. The differences relate to the description of the initial channel. The EIS describes the situation only at long internuclear distances as an eikonal perturbation [see Eq. (2.16) above], and since the peak is shifted towards lower energies, one can interpret this situation as a *binding* energy. The IA, on the other hand, better describes the internal region, permitting also the distortion of the "fast" electrons [see Eq. (2.5) above]. The outcome seems to indicate an *antibinding* effect which moves the enhancement towards higher electron energies. Experiments would be welcome to test the IA prediction. Departure from the Z_P^2 behavior, as discussed before, should be seen in the context of the entire peak.

C. Shift of the binary peak

Now we turn our attention to the shift

$$\Delta=\tfrac{1}{2}(2v)^2-\tfrac{1}{2}(k_{TM})^2 , \tag{4.1}$$

where k_{TM} is the momentum where the binary peak is maximal. It is interesting to note that even though the theoretical peaks seem very close to each other, Δ may be rather different, indicating that the shift is a quite sensitive quantity. Besides the intrinsic binding energy of the initial state, which shifts the position in relation to $2v^2$, two other sources are examined next.

It the target is hydrogenlike ($Z_T=\sqrt{-2\varepsilon_i}$, ε_i being the binding energy of the initial state) and the Z_P^2 behavior holds, then, by using the scaling properties of the Schroedinger equation, the shift can be displayed in a universal plot of $\Delta/|\varepsilon_i|$ versus $\frac{1}{2}v^2/|\varepsilon_i|$. Figure 3(a) shows the universal curve U, obtained with the simple PW approximation (see the Appendix). The theoretical prediction differs from the experimental results. We can

proceed further and present the Compton profile better. For helium atoms, that profile can be easily computed by using Clementi-Roetti Hartree-Fock wave functions.[19] Some improvement is observed when a single z function, curve $1Z$, and multiple z functions, curve $5Z$, are used, as shown in Fig. 3(b) (the $2Z$ function does not introduce appreciable differences relative to the $5Z$ one). We conclude that the shift Δ seems to be quite sensitive to the description of the initial wave function. Still, the simple PW model does not fully explain the experimental shift.

As indicated before, the previous study does not consider the influence of the projectile. For large Z_P, the maximum of the peak is expected to be shifted. The use of the EIS, instead of the simple PW, introduces substantial agreement with the data, as shown in Fig. 3(b). The tendency and magnitude of the experiments are now reasonably described if the errors of the experiments are considered. The EIS approaches the PW, as the velocity increases, as expected.

The use of the IA to calculate Δ is very expensive in computing time. For $Z_P \leq 9$, its shift (not shown) approximately equals the EIS shift. However, for large Z_P, the shift is even less than the PW shift.

Two main conclusions should be drawn from the present discussion: first, the position of the peak varies with the Compton profile used, and second, for relatively large projectile charges the binary encounter peak is further shifted. These effects seems to be quite important if we are interested in a *quantitative* description of the binary encounter peak, even though such features are not immediately apparent from the DDCS.

V. RIDGE OR $v/2$ ELECTRONS

It is well known that electron spectra exhibit two cusps, namely, the ECC one at the projectile velocity $k_p=0$ (or $\mathbf{k}_T=\mathbf{v}$) and another one at $k_T=0$ (or $\mathbf{k}_P=-\mathbf{v}$) corresponding to electrons at rest with respect to the target. It has been found experimentally[22] that there is also a ridge in the electron distribution between these cusps. Although later measurements showed that the ridge is less prominent than first measured,[23] it is still observed as an enhancement of the electron distribution in the forward direction. It should be remarked that we do not mean electrons with a precise velocity $v/2$ or any other preferable velocity arising from the saddle region, where the derivatives of the combined projectile and target potentials cancel. These saddle electrons[24] would travel in the neighborhood of the equiforce or saddle point, which changes with the target and projectile charges.

Figure 4 displays the DDCS for helium ionization in the forward direction for electron velocities in between

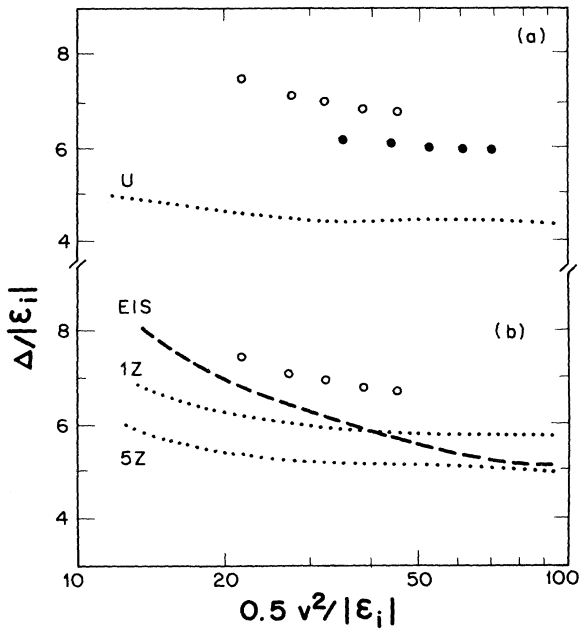

FIG. 3. Scaled shift $\Delta/|\varepsilon_i|$ vs the scaled kinetic impact energy $\frac{1}{2}v^2/|\varepsilon_i|$ where ε_i is the binding energy of the electron ($\varepsilon_i=-0.918$ for He and $\varepsilon_i=-0.567$ for H_2). Open and solid cirlces are the experiments corresponding to F^{9+} on He and H_2, respectively. Dotted curve U denotes the PW approximation using a target charge in the initial electronic state given by $Z_T=\sqrt{2|\varepsilon_i|}$ (i.e., $Z_T=1.35$ for He and 1.065 for H_2). Dotted curves labeled $1Z$ and $5Z$ are results with the PW approximation using a single ($Z_T=1.687$) and multiple z function of Clementi and Roetti,[19] respectively. The dashed line denotes the EIS calculation for F^{9+} on helium.

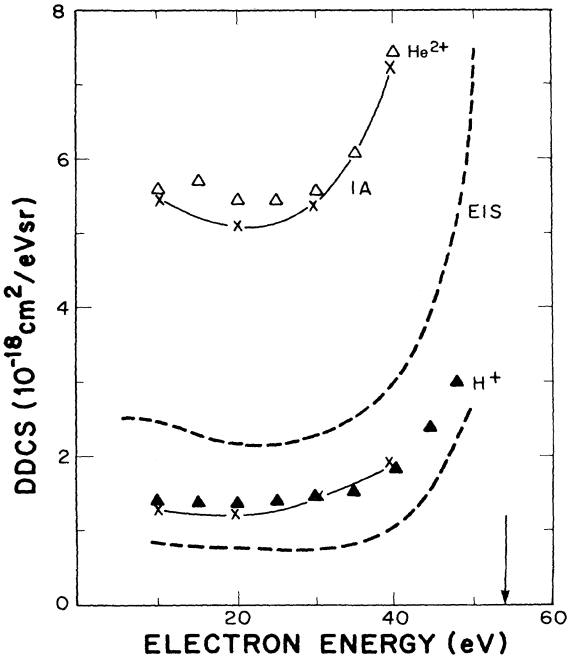

FIG. 4. Double-differential cross sections in the forward direction ($\theta_e=0$) for ionization of helium by impact of He^{2+} and H^+ as a function of the ejected electron energy. The impact energy is in both cases 100 KeV/amu ($v=2$). All quantities are in the target reference frame. Theory as in Fig. 1. Open and solid triangles are the experiments of Bernardi *et al.*[25] corresponding to He^{2+} and H^+ impact, respectively. The arrow indicates the position of th ECC cusp.

the projectile and target nucleus one. The IA gives a very good description of the two sets of data,[25] corresponding to H^+ and He^{2+} projectiles at the same impact velocity ($v=2$). The EIS moderately follows the proton results, but, as for any perturbative method, breaks down as Z_P increases. The IA, on the other hand, seems to cope quite well with $Z_P=2$, indicating that this theory may be adequate to deal with multicharged ions.

Now, we investigate the ridge region of the DDCS, i.e., the region near 0° between the $k_T=0$ and $K_T=v$ cusps. To that end, we extend the electron angular range. As indicated in Sec. III, for electron angles other than 0° or 180°, an additional integration on the projectile azimuth is needed, which would involve an undesirable amount of computing time. Since we are interested in small electron angles, the following approximation was made:

$$\frac{d\sigma}{dE_e d\Omega_e} \sim 2\pi \frac{d\sigma}{dE_e d\Omega_e d\varphi}(\varphi-\varphi_e=\pi/2) , \tag{5.1}$$

which is equivalent to one-point integration with a Gauss quadrature. Equation (5.1) is correct for $\theta_e=0°$ *or* 180°, and it should be quite accurate for the small angles used here.

Figure 5 shows DDCS as a function of the ejection angle for two electron energies, 20 and 40 eV, corresponding to the ridge region. The system here under consideration is protons on helium at 100-keV impact energy. The IA is compared with three sets of experiments[25,26] and the agreement is very satisfactory (in fact, better than expected if we take into account the fact that we are using an approximate wave function for the final continuum state of helium[20]). The ridge is not spectacular but is observable. The ridge is present at 20 eV corresponding to $k_T=1.21$ a.u. $\approx v/2$ in both the IA and EIS theories. In contrast, for the Born theory with target eigenstates, the cross section has a minimum at 0°. Dettman's first-order theory and similar theories which employ plane-wave initial state and the final state of Eq. (2.1) naturally obtain

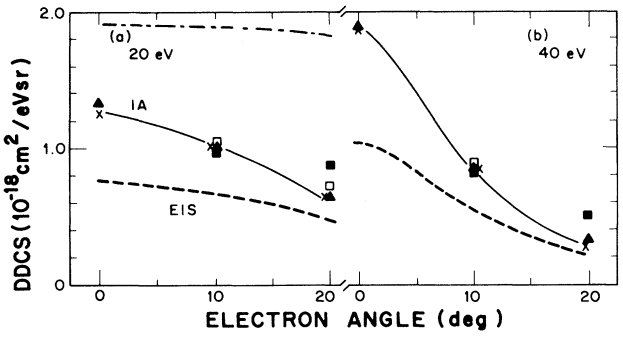

FIG. 5. Double-differential cross sections for ionization of helium by impact of H^+ as a function of the ejected angle θ_e. (a) and (b) show results for 20 and 40 eV electron energies, respectively. The proton energy is 100 KeV/amu ($v=2$). All quantities are in the target reference frame. Theory as in Fig. 1, with the dot-dash curve representing a calculation with a plane-wave initial state. Solid triangles are the experiments of Bernardi *et al.*,[25] solid and open quadrangles are data from Rudd *et al.*[26]

the ECC cusp, but do not usually obtain a ridge. For interpretive purposes, we considered an approximation[15] using the final state of Eq. (2.1) and plane-wave initial states in the ridge region. For 20-eV electrons, we obtained the distribution given by the dot-dash curve in Fig. 5(a). The distribution is essentially flat between 0° and 10°, and decreases slightly at 20°. In contrast, the IA and EIS show a more noticeable ridge structure, although the ridge is less pronounced for the EIS. Also, note that the absolute value is in poor agreement with experiment when plane-wave initial states are used.

In this paragraph we attempt to give some explanation as to why the ridge extending to the $v/2$ region is most prominant in the IA, less prominant in the EIS, and not present in simple first-order theories. In a multiple-scattering interpretation, we consider two steps. The electron is first "boosted" to some intermediate state and this is described by the initial wave function. Then, the electron is "guided" by the final potential. Provided that the final state includes the effects of *both* centers [as in our Eq. (2.1)], the electron distribution is expected to describe the ECC cusp and also to narrow in the direction perpendicular to the beam to produce the ridge, as explained in Ref. 22. Certainly, the IA initial state [Eq. (2.5)], which better describes the short *P-e* distances, seems to boost the electron appropriately in the first step. The EIS initial state [Eq. (2.17)], describing only the long *P-e* distances, seems to boost electrons with lower probability. Compare this mechanism for the two theories applied to $1s$-$1s$ charge transfer as opposed to the $1s$-$k_P l$ charge transfer relevant here. For $1s$-$1s$ charge transfer the peaked IA includes a term $(\mathbf{P}^2-v^2-2iZ_T v)^{-1}$ that describes the Thomas double-collision mechanism. The corresponding peaked EIS has an approximate form of this term, namely, $(-v^2-2iZ_T v)^{-1}$; thus it lacks the Thomas peak but does incorporate the double-collision mechanism, although with lower probability than does the IA. The presence of a ridge extending to the $v/2$ region is therefore completely consistent with the multiple-scattering interpretation. Although this analysis is given within the high-energy distorted-wave formalism, a similar analysis holds in the low-energy molecular formalism.[27]

VI. ECC CUSP OR v ELECTRONS

Regarding the ECC cusp, there are a series of interesting features that we would like to investigate (for a good review on the subject, see Ref. 28). We would like to concentrate on two points, namely, shape and magnitude. As is well known,[16] the main behavior of the cusp is ascribed to the Coulomb factor around the projectile:

$$|\gamma(a_P)|^2=\frac{2\pi a_P}{1-\exp(-2\pi a_P)} \rightarrow 2\pi a_P \quad \text{as } a_P \rightarrow \infty . \tag{6.1}$$

So to get more insight, we define a "normalized" DDCS, as follows:

$$\frac{d\sigma^N}{dE_e d\Omega_e} = \frac{1}{|\gamma(a_P)|^2} \frac{d\sigma}{dE_e d\Omega_e} , \tag{6.2}$$

which is plotted is Fig. 6 and compared with the corresponding experimental quantity for 100-keV amu H^+ and He^{2+} on helium in the forward direction. We do not extend the data very near to the ion velocity to avoid dealing with the experimental angular resolution, which is known to be decisive for the yield at the cusp.[16] The IA accounts for the experiments in magnitude and shape, except in the forward direction for He^{2+} impact, where it seems to underestimate the data, for unknown reasons. Note that the asymmetry of the cusps, i.e., more electron production for $k_T < v$ than for $k_T < v$, is quite well explained by the IA. On the contrary, the EIS seems to have the wrong asymmetry for He^{2+} impact.

By introducing the most elementary parametrization of the cusp,[28]

$$\frac{d\sigma^N}{dE_e d\Omega_e} \sim B_0^0(1+\beta_1 \cos\theta_P) , \tag{6.3}$$

where θ_P is the electron ejection angle relative to the beam direction in the projectile frame, we find that

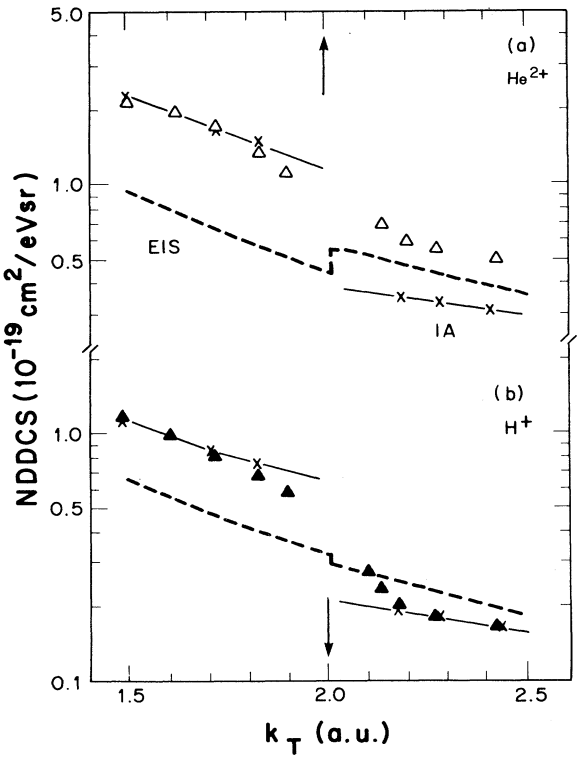

FIG. 6. Double-differential cross sections normalized to the projectile Coulomb factor [see Eq. (6.2)] in the forward direction ($\theta_e = 0$) for ionization of helium by impact of (a) He^{2+} and (b) H^+ as a function of the ejected electron momentum. The impact energy is in both cases 100 KeV/amu ($v = 2$). All quantities are in the target reference frame. Theory as in Fig. 1. Open and solid triangles are the experiments of Bernardi *et al.*[25] corresponding to He^{2+} and H^+ impact, respectively. The arrow indicates the position of the ECC cusp.

$$B_0^0 = \frac{d\sigma_+^N + d\sigma_-^N}{2} \quad \text{and} \quad \beta_1 = \frac{d\sigma_+^N - d\sigma_-^N}{d\sigma_+^N + d\sigma_-^N} . \tag{6.4}$$

$d\sigma_{+,-}^N$ are the normalized cross sections for $\theta_P = 0°$ and 180°, respectively, i.e., in the forward and backward directions with respect to the cusp. For proton impact, we can estimate *very roughly* from Fig. 6 that $d\sigma_+^N$ and $d\sigma_-^N$ are of the order of 0.2×10^{-19} and 0.7×10^{-19} cm^2/eV sr to give a dipole parameter $\beta_1 \sim -0.55$, which compares quite well with the experimental values, -0.75 and -0.65, of Lucas and Steckelmacher[28] and Dahl,[29] respectively for details, see Fig. 8 of Ref. 28). Similar evaluation for He^{2+} impact gives $\beta_1 \sim -0.47$. The IA seems to be a successful theory for analyzing the details of the ECC cusp with the above parametrization technique.

VII. BACKWARD DIRECTION

In this section we deal with the DDCS at backward electron angles i.e., when the electron is ejected opposite to the beam direction. For ejection angle 180° in the target frame, the integration on the projectile azimuthal angle is again straightforward, and for slightly smaller angles, approximation (5.1) can be used with confidence. In this region Auger peaks are expected to be observed more clearly because the direct ionization yield is small.

To our knowledge, no experimental cross section in the present range of interest has been published using pure hydrogenic targets; therefore, we compare again with experiments performed with helium targets. A comprehensive study of helium ionization by impact of protons at large angles was published some years ago by Manson *et al.*[30] In that experimental and theoretical work, the authors compared the experiments with the first Born approximation as a direct process calculated within the independent-electron model with Hartree-Slater wave functions for the discrete initial and continuum final state. Two important conclusions were drawn: first, the discrepancy of the first-order theory with the data in the forward direction was correctly assigned to the capture to the continuum mechanism. Second, the very good agreement of the theory with the data at very large ejection angles was ascribed to the use of an adequate final continuum state which accounts for the passive electron. Previous results of Oldham,[31] using a simple hydrogenic continuum state, exhibited very large discrepancies at very large angles. At this stage we have to remark that the T-e interacting part, namely, $\psi^-(Z_T, \mathbf{k}_T|\mathbf{r}_T)$ in our final state Ψ_f^P in Eq. (2.1), is here also described by a simple hydrogenic continuum state with an effective charge $Z_T = 1.687$. The inclusion of the Hartree-Slater final wave function is, of course, possible, with the corresponding increasing in the cost of computing time.

Fig. 7 shows DDCS versus electron energy for 100-keV protons on helium for ejection angles 180° and 160°. As usual, the crosses denote the IA calculations and the dashed line, the EIS. Figure 7 also shows three sets of experiments by Rudd *et al.*[26] The structure at 35 eV is due to autoionization of the double excited states, which is not accounted for in the present formalism. The EIS underestimates the data while the IA describes them quite

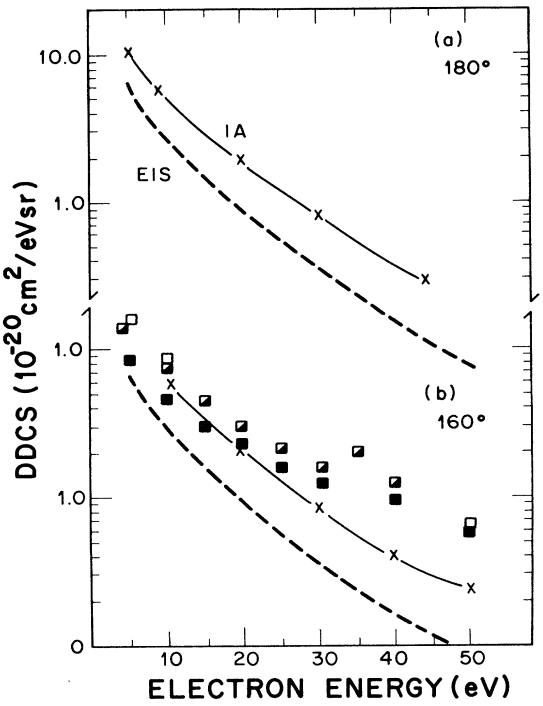

FIG. 7. Double-differential cross sections at large angles for ionization of helium by impact of 100-KeV H^+ as a function of the ejected electron energy. (a) and (b) correspond to electron angles $\theta_e = 180°$ and $\theta_e = 160°$ respectively. All quantities are in the target reference frame. Theory as in Fig. 1. Open, solid, and half-solid quadrangles are the experiments of Rudd *et al.* (Ref. 26).

well up to 20 eV. Beyond that, the IA also falls below experiment. For proton impact, the IA is very close to the first-order Born approximation (dot-dashed line in Fig. 8), calculated with the same initial and final *T-e* functions. In accordance with Manson *et al.*,[30] we expect our IA to improve when the effect of the passive electron is built into the final continuum wave function.

Backward ejection angles by impact of multicharged ions would provide an important probe of the physics of the problem. Figure 8 anticipates some results of interest in relation to ionization of helium by impact of He^{2+}, Li^{3+} and p^- (antiprotons). The first-order Born approximation is well known to behave as Z_P^2 times the corresponding value for proton impact (see dot-dashed line in Fig. 8). However, the IA departs from the Z_P^2 rule and saturation effects are observed. Also, the IA predicts that antiprotons with $Z_P = 1$ produce more electrons than do protons, particularly at low electron energies. The proton and antiproton DDCS approach a common value as the electron velocity increases, indicating that the mechanism that produces high-energy electrons is a single collision with the projectile.

ACKNOWLEDGMENTS

This research has been sponsored by the U.S. Department of Energy, under Contract No. DE-AC05-84OR21400 with Martin Marietta Energy Systems, Inc.

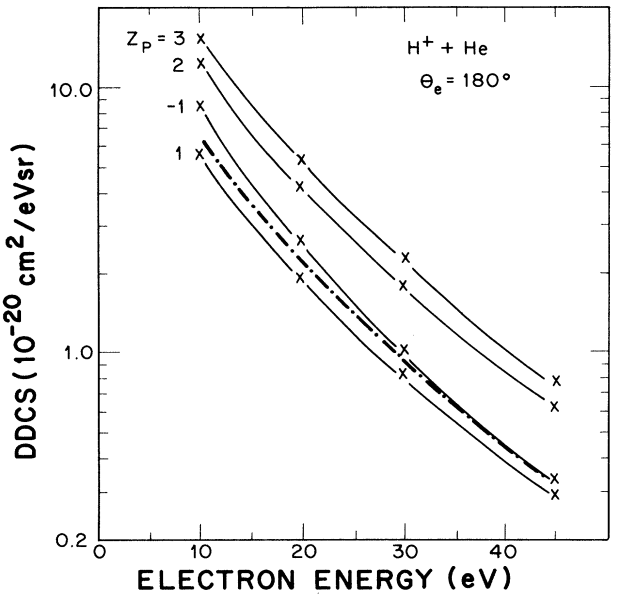

FIG. 8. Double-differential cross sections in the backward direction ($\theta_e = 180$) for ionization of helium by impact of 100-KeV H^+, He^{2+}, Li^{3+}, and p^- (antiprotons) as a function of the ejected electron energy. All quantities are in the target or laboratory reference frame. Theory as in Fig. 1, and dot-dashed line is the first Born approximation considered as a direct process.[15]

APPENDIX: PLANE-WAVE APPROXIMATION

The plane-wave approximation is the simplest quantum model for ionization. The final state is described by plane waves affected by neither the target nor the projectile, and the initial state is the unperturbed first-order Born wave functions. After simple algebra, one finds that the T matrix is given by[14]

$$T_{\mathrm{PW}} = \frac{1}{(2\pi)^{3/2}} \tilde{V}_P(\mathbf{P}) \tilde{\phi}_i(\mathbf{k}_T - \mathbf{P}) \ . \tag{A1}$$

The DDCS can be rewritten, for convenience, as

$$\frac{d\sigma}{dE_e d\Omega_e} = \frac{2\pi k_T}{v^2} \int d\mathbf{P} |\tilde{V}_P(\mathbf{P}) \tilde{\phi}_i(\mathbf{k}_T - \mathbf{P})|^2 \delta(P_z - P_m) \ , \tag{A2}$$

where $P_m = (0.5k_T^2 + |\epsilon_i|)/v$ is the minimum momentum transfer and ϵ_i is the initial binding energy. If the electron is initially in the ground state and it is ejected in the forward direction $\theta_e = 0$, the corresponding DDCS has a simple closed form given by

$$\frac{d\sigma_{\mathrm{PW}}}{dE_e d\Omega_e} = \frac{2^5 Z_T^5 Z_P^2 k_T}{\pi v^2 P_m^{10}} F(\xi) \ , \tag{A3}$$

where

$$F(\xi) = \left[\frac{1}{\xi} + \frac{22}{3\xi^2} + \frac{10}{\xi^3} + \frac{4}{\xi^4} \right] \frac{1}{(1+\xi)^3} - \frac{4}{\xi^5} \ln(1+\xi) \ , \tag{A4}$$

$$\xi=\frac{(Z_T^2-P_m^2)+(k-P_m)^2}{P_m^2} . \tag{A5}$$

In order to make a comparison with the classical binary theory, we approximate: $\tilde{V}_P(\mathbf{P})\sim\tilde{V}_P(P_m)$ in Eq. (A2), so the DDCS can be written, for any θ_e, as

$$\frac{d\sigma_{\rm PW}}{dE_e d\Omega_e}\sim\left[\frac{4k_T}{v^2P_m^4}\right]Z_P^2J_i(\hat{\mathbf{v}}\cdot\mathbf{k}_T-P_m) , \tag{A6}$$

where J_i is the so-called Compton profile

$$J_i(u_{z0})=\int d\mathbf{u}|\tilde{\phi}_i(\mathbf{u})|^2\delta(u_z-u_{z0}) . \tag{A7}$$

Equation (A6) has a structure similar to the classical theory [Ref. 8, Eq. (6)]. When $k_T\sim 2v\gg|\epsilon_i|$, the term in square brackets in Eq. (A6) tends to the same limit as the classical counterpart. Further, for the cases studied in Ref. 8 we have found no appreciable differences in the vicinity of the binary peak between the present quantum plane-wave DDCS, Eq. (A6), and the classical model.[8] Also, it can be proven that the first Born approximation with target eigenstates[15] approaches very closely the PW values around the binary encounter peak, at large impact velocities ($v\gg 10Z_T$).

*On sabbatical leave from Instituto de Astronomia y Fisica del Espacio, Casilla de Correo No. 67, Sucursal 28, 1428 Buenos Aires, Argentina.

[1]A. Salin, J. Phys. B **2**, 631 (1969).

[2]J. Macek, Phys. Rev. A **1**, 235 (1970).

[3]I. Cheshire Proc. Phys. Soc. **84**, 89 (1964).

[4]D. R. Belkic, J. Phys. B **11**, 3529 (1978); **13**, L589 (1980).

[5]C. R. Garibotti and J. E. Miraglia, Phys. Rev. A **21**, 572 (1980); J. Phys. B **14**, 863 (1981).

[6]D. S. F. Crothers and J. F. McCann, J. Phys. B **16**, 3229 (1983).

[7]C. O. Reinhold, C. Falcon, and J. E. Miraglia, J. Phys. B **20**, 3737 (1987); see also R. E. Olson, C. O. Reinhold, and D. R. Shultz (unpublished), and references therein.

[8]D. H. Lee, P. Richard, T. J. M. Zourus, J. M. Sanders, J. L. Sinpaugh, and H. Hidmi, Phys. Rev. A **41**, 4816 (1990).

[9]V. Rodriguez and J. E. Miraglia, Phys. Lett. **138A**, 123 (1989); Phys. Rev. A **39**, 6594 (1989).

[10]B. Brendle, R. Gayet, J. P. Rozet, and K. Wohrer, Phys. Rev. Lett. **54**, 2007 (1985); see also K. Reymann, K. H. Schartner, B. Sommer, and E. Trabert, Phys. Rev. A **38**, 2290 (1988).

[11]G. F. Chew, Phys. Rev. **80**, 196 (1950); see also M. R. C. McDowell and J. P. Coleman, *Introduction to the Theory of Ion-Atom Collisions* (North-Holland, Amsterdam, 1970). A derivation that obtains the IA from the distorted-wave strong-potential Born approximation is given in J. Macek and K. Taulbjerg, Phys. Rev. A **39**, 6064 (1989).

[12]M. S. Gravielle and J. E. Miraglia, Phys. Rev. A **38**, 5034 (1988).

[13]V. D. Rodriguez and J. E. Miraglia, in *Proceedings of the XVI International Conference on the Physics of Electronic and Atomic Collisions, New York, 1989,* AIP Conf. Proc. No 205, edited by A. Dalgarno, R. S. Freund, M. S. Lubell, and T. B. Lucatorto (AIP, New York, 1990), p. 490; (unpublished).

[14]J. E. Miraglia and V. H. Ponce, J. Phys. B **13**, 1195 (1980).

[15]D. R. Bates and G. Griffing, Proc. Phys. Soc. London Sect. A **66**, 961 (1953).

[16]K. Dettmann, K. G. Harrison, and M. W. Lucas, J. Phys. B **7**, 269 (1974).

[17]J. E. Miraglia, J. Phys. B **16**, 1029 (1983).

[18]P. D. Fainstein, V. H. Ponce, and R. D. Rivarola, J. Phys. B **21**, 287 (1988); **21**, 2989 (1988); **22**, 1207 (1988).

[19]C. Clementi and C. Roetti, At. Data Nucl. Data Tables **14**, 445 (1974), Table I.

[20]This latter choice is perhaps the more doubtful. Alternatively, one could use a hydrogen continuum wave function ($Z_T=1$) to satisfy the asymptotic condition, but it does not describe the internal region where the main contribution to the matrix element comes from.

[21]P. Richard, D. H. Lee, T. J. M. Zourus, J. M. Sanders, and J. L. Shinpaugh, J. Phys. B (to be published).

[22]W. Meckbach, P. J. Focke, A. R. Goni, S. Suarez, J. Macek, and M. G. Menendez, Phys. Rev. Lett. **57**, 1587 (1986).

[23]G. Bernardi, S. Suarez, P. Focke, and W. Mechbach, in *Proceedings of the Third Workshop on High-Energy Ion-Atom Collisions, Debrecen, Hungary, 1987,* edited by D. Berenyi and G. Hocks, Lecture Notes in Physics Vol. 294 (Springer-Verlag, Berlin, 1988), p. 295.

[24]V. D. Irby, T. J. Gay, J. W. Edwards, E. B. Hale, M. L. McKenzie, and R. E. Olson, Phys. Rev. A **37**, 3612 (1988).

[25]G. Bernardi, S. Suarez, P. D. Fainstein, C. R. Garibotti, W. Meckbach, and P. Focke, Phys. Rev. A **40**, 6863 (1989); (private communication).

[26]M. E. Rudd, L. H. Toburen, and N. Stolterfoth, At. Data Nucl. Data Tables **18**, 413 (1976). These authors estimated their experimental uncertainties at 20% for electron energies larger than 20 eV, 40% at 10 eV, and a factor of 2 or more at lower energies.

[27]See, for example, S. Y. Ovchinnikov and E. A. Solovev, Comments At. Mol. Phys. **22**, 69 (1988). According to modern ideas, the slow-collision ionization mechanism may be seen also as two-step processes: On the way in, the particles approach each other via a certain molecular state; then at intermediate distances, the electron crosses to a state, in which, on the way out, it is promoted to the continuum via a lengthy series of pseudocrossings passing through the Rydberg states. In our case, the ingoing and outgoing mechanisms are described by the initial and final wave functions, respectively.

[28]M. W. Lucas and W. Steckelmacker, *Proceedings of the Third Workshop on High-Energy Ion-Atom Collisions, Debrecen, Hungary 1987* (Ref. 23), p. 295.

[29]P. Dahl, J. Phys. B **18**, 1181 (1985).

[30]S. T. Manson, L. H. Toburen, D. H. Madison, and N. Stolterfoth, Phys. Rev. A **12**, 60 (1975).

[31]W. J. B. Oldahm, Phys. Rev. **140**, A1477 (1965).